Novel contribution on the diagenetic physicochemical features of bone and teeth minerals, as substrates for ancient DNA typing

A. Grunenwald · C. Keyser · A. M. Sautereau · E. Crubézy · B. Ludes · C. Drouet

Abstract The extraction of DNA from skeletal remains is a major step in archeological or forensic contexts. However, diagenesis of mineralized tissues often compromises this task although bones and teeth may represent preservation niches allowing DNA to persist over a wide timescale. This exceptional persistence is not only explained on the basis of complex organo-mineral interactions through DNA adsorption on apatite crystals composing the mineral part of bones and teeth but is also linked to environmental factors such as low temperatures and/or a dry environment. The preservation of the apatite phase itself, as an adsorption substrate, is another crucial factor susceptible to significantly impact the retrieval of DNA. With the view to bring physicochemical evidence of the preservation or alteration of diagenetic biominerals, we developed here an analytical approach on various skeletal specimens (ranging from ancient archeological samples to recent forensic specimens), allowing us to highlight several diagenetic indices so as to better apprehend the complexity of bone diagenesis. Based on complementary techniques (X-ray diffraction (XRD), Fourier transform infrared (FTIR), calcium and phosphate titrations, SEM-EDX, and gravimetry), we have identified specific indices that allow differentiating 11 biological samples, primarily according to the crystallinity and maturation state of the apatite phase. A good correlation was found between FTIR results from the analysis of the $\nu_3(PO_4)$ and $\nu_4(PO_4)$ vibrational domains and XRD-based crystallinity features. A maximal amount of information has been sought from this analytical approach, by way of optimized posttreatment of the data (spectral subtraction and enhancement of curve-fitting parameters). The good overall agreement found between all techniques leads to a rather complete picture of the diagenetic changes undergone by these 11 skeletal specimens. Although the heterogeneity and scarcity of the studied samples did not allow us to seek direct correlations with DNA persistence, the physicochemical parameters described in this work permit a fine differentiation of key properties of apatite crystals among post mortem samples. As a perspective, this analytical approach could be extended to more numerous sets of specimens so as to draw statistical relationships between mineral and molecular conservation.

Keywords Bone · Teeth · Diagenesis · Ancient DNA · Apatite · Carbonate content · FTIR · Crystallinity

A. Grunenwald A. M. Sautereau C. Drouet (✉)
CIRIMAT Carnot Institute – Phosphates, Pharmacotechnics, Biomaterials, University of Toulouse, CNRS/INPT/UPS, ENSIACET, 4 allée Emile Monso, 31030 Toulouse Cedex 4, France
e-mail: christophe.drouet@ensiacet.fr

A. Grunenwald · C. Keyser
Institute of Legal Medicine, AMIS Laboratory, CNRS UMR 5288, University of Strasbourg, 11 rue Humann, 67085 Strasbourg Cedex, France

E. Crubézy
Molecular Anthropology and Image Synthesis Laboratory (AMIS), CNRS UMR 5288, University of Toulouse, 37 allées Jules Guesde, 31000 Toulouse, France

B. Ludes
Institute of Legal Medicine, Paris Descartes Medicine Faculty, Paris Descartes University, 15 Rue de l'Ecole de Médecine, 75006 Paris, France

Introduction

Deciphering characteristics of extinct organisms and their environment from the preserved features of archeological bone and teeth samples is a challenging task. Valuable data about biological schemes (e.g., concerning diet, climate, etc.) can be retrieved from isotopic or trace elements composition of both the collagenic and mineral parts of skeletal specimens, provided that this composition remains essentially unchanged

over time [1–3]. Molecular preservation could also occur to the point where minute amounts of DNA, as well as peptide fragments, may be extracted and sequenced (e.g., [4–7]). However, diagenesis amends in various manners the physicochemical and molecular features of the skeletal remains, once in their burial environment. In such cases, the authenticity of the biogenic signals may no longer be ascertained and ancient DNA typing may become very problematic or even unrealizable. Nonetheless, ancient DNA studies could successfully be undergone using, as starting materials, some fragments or pieces of skeleton arising from various archeological or forensic research contexts, with a large spatiotemporal distribution, from cold or even temperate environments, over a period of about 600,000 years (e.g., [8–12]).

Therefore, the mechanisms explaining how ancient DNA can be preserved into the sample, and how the biogenic signals could be modified, have to be elucidated. Bone diagenesis mainly depends on three factors: (i) the nature of the skeletal tissue, with emphasis given on the mineral–organic interactions underlying degradation pathways, (ii) the chemistry of the sediments (presence of water, pH, ionic strength, oxidation–reduction potential, etc.), (iii) and physical parameters, especially temperature which is the main factor explaining DNA alteration. Moreover, potential pitfalls of ancient DNA studies result from contamination with modern DNA or coextracted PCR inhibitors.

Among mineralized tissues, compact bone and dentin usually provide the "best" ancient DNA in terms of fragment length, amount, and chemical modifications [13–15]. The mineral phase of both compact bone and dentin is commonly described by a poorly crystalline nonstoichiometric carbonated apatite, representing almost 70 wt.% of the tissue. By contrast, teeth enamel is far much mineralized with 97 wt.% of the composition represented by hydroxyapatite microcrystals resembling closely stoichiometric hydroxyapatite (HA, $Ca_{10}(PO_4)_6(OH)_2$). Given the greater thermodynamic stability of stoichiometric HA as compared with nonstoichiometric apatites [16], the enamel material is the most resistant tissue toward diagenetic changes, although substitutions occur in the form of exogenous carbonation and incorporation of traces elements. Contrariwise, bone and dentin mineralization are composed of nonstoichiometric apatite nanocrystals exhibiting a lower thermodynamic stability associated to a greater reactivity. In particular, the surface features are governed by the presence of a very reactive non-apatitic outer layer (containing both ions and water molecules) [17–20], typically leading to a 60-fold greater specific surface area compared with enamel crystals. This non-apatitic hydrated layer is metastable and contains labile ions (Ca^{2+}, HPO_4^{2-}, CO_3^{2-}, etc.) [21, 22]. It thus plays a significant role in ionic exchanges or molecular adsorption processes [23–27]. This exceptional reactivity is thought to act as a premise in DNA adsorption onto apatite crystals, leading to its long-term preservation [12, 28–31].

The physicochemical processes of apatite diagenesis occur in several stages, driven by thermodynamic stability and solid-solution equilibrium laws [32]. First of all, the metastable non-apatitic hydrated layer progressively disappears during a spontaneous maturation phenomenon, favoring the progressive incorporation of surface labile ions into the apatite core of the nanocrystals (this spontaneous character of apatite maturation has recently been experimentally quantified by Rollin-Martinet et al. [16]). Taking into account the wide substitution possibilities offered by the apatite structure, this may then lead to a significant modification of the apatitic phase composition, with not only the incorporation of ionic species from the hydrated layer, but also possibly that of ions found in the immediate surroundings. This process could then reoccur over the whole taphonomic history of the sample, together with the dissolution–recrystallization of the crystals, whether due to micro-organism activity or to the chemistry of surrounding fluids [32, 33]. In a similar way, the evolution of biological apatites toward a greater stability state may also explain the frequent occurrence of fluorine-rich carbonated hydroxyapatite (francolite) among very old samples [34]. In addition to these chemical modifications, Ostwald ripening (preferential formation of larger, less soluble crystals at the expense of the dissolution of the smallest ones) may also contribute to the changes observed in skeletal specimens during diagenesis [32].

Given the potential protective role of apatite toward DNA, a detailed review of the diagenetic changes of the mineral phase may prove helpful to evaluate the level of bone/tooth alteration, and possibly to predict the preservation state of DNA within old samples. Thus far, a better understanding of diagenetic changes is only achievable by means of extensive physicochemical characterizations using complementary techniques [35]. However, this task is complicated by the composite nature of biological hard tissues, potentially modified by a wide range of diagenetic events, and the small to very small quantities of material available for investigations.

In the present work, a series of physicochemical characterization methods have been used and adapted to the examination of diagenetic specimens. Given the small number of collected samples, arising from a wide variety of spatial and temporal sources (which is frequently the case when dealing with archeological materials), no attempt has been made to express our results in a statistical point of view. We rather focus here on the type of physicochemical information that may be drawn from the use of materials science techniques and of apatite investigation protocols that were already implemented in the field of bone-related biomaterials. The results of the characterization of a dozen of samples arising from various archeological and forensic contexts—which allowed or not DNA extraction—have been studied in order to relate them

with the diagenetic patterns generally observed during the course of taphonomic history. When judged adequate, we then point out some general tendencies noticed among the samples.

Materials and methods

Skeletal specimens analyzed in this work

In this study, ten bone and teeth specimens (listed in Table 1) originating from diverse geographical areas (for archeological samples, see Fig. 1) and corresponding to a wide datation range (from immediately post mortem to Iron Age) were investigated. The samples were provided by the AMIS laboratory (CNRS, UMR 5288, France) which is involved in ancient DNA studies.

To eliminate surface contamination, the outer surface of the bones was abraded to a depth of 2–3 mm with a sanding machine whereas the teeth were cleaned with bleach, rinsed with ultrapure water, and exposed to UV light for 30 min on each side. Cortical bone pieces and whole teeth were then powdered in a grinder mill under liquid nitrogen using a 6870 SamplePrep Freezer Mills (Fischer Bioblock, Illkirch, France). For each sample, an aliquot of this milled fraction was then subjected to a second milling process (Spex 5710 Freezer Mill) in order to yield finer powdered samples necessary for the physicochemical characterizations.

Synthetic biomimetic apatites used as references

When mentioned in the text, two well-characterized synthetic apatite samples with biomimetic features were used for comparative purposes. These samples were synthesized by double decomposition starting from calcium nitrate and ammonium hydrogenphosphate (in the additional presence of sodium bicarbonate for the carbonated sample) and matured 1 week in solution, prior to filtering on Büchner funnel, washing with deionized water, and freeze-drying. The complete procedure is available in detail in our previous reports [18, 36]. The carbonated and noncarbonated samples will be referred to in the text as "1w-hac" and "1w-hap."

DNA extraction and amplification

DNA extraction was carried out according to [37]. Fifteen autosomal STRs (D8S1179, D7S820, D3S1358, D13S317, D16S539, D2S1338, D19S433, D5S818, D21S11, CSF1PO, vWA, THO1, TPOX, D18S51, and FGA) and the sex-determining marker amelogenin were then amplified using the AmpFlSTRs Identifiler Plus™ kits (Applied Biosystems). PCR conditions were those recommended by the manufacturer except that 34 cycles were used instead of 28. Amplified products were analyzed on a 3500 Genetic Analyzer (Life Technologies) using the GeneMapper 4.1 software (Life Technologies).

Physicochemical characterization

The amount of organic (mostly collagenic) fraction of the skeletal specimens was estimated by weighing the dried insoluble residue remaining after acidic treatment with $HClO_4$ 6 M (1 ml for 25 mg of sample; deionized water, 25 ml) until no mineral aggregates were observable. The supernatant was collected by filtration with Acrodisc® syringe filters with

Table 1 List of bone and teeth samples, with epoch, type, and provenance location

No.	Epoch	Type	Gender/age	Burial site	DNA	Additional information
1	Modern	Femur	Male/57 years old	None	n.t.	Frozen sample after autopsy
2	Modern/forensic	Femur	Female/88 years old	Unknown	n.t.	Surface decomposition, post mortem delay of 3 months
3a	Modern/forensic	Bone	Male	20 years in water	−	Surface sampling of the bone
3b					++	Deep sampling of the bone
4	Iron Age[a]	Bone	Female	Krasnoyarsk region, Russia Egyin Gol	+	S09 [8]
5	Iron Age[b]	Vertebra	Male/adult	Necropolis, Mongolia	+	Grave no. 17. Excavated in late the 1990s [60]
6	Iron Age[b]	Long bone	Unknown	Egyin Gol Necropolis	−	Grave no. 34
7	Third–eleventh century BC	Tooth	Unknown	Atacama desert, Chile	−	Solcor site (Sol 14), pre-Incaic era [61]
8	Middle Age	Tooth	Male/adult	Roeschwoog Alsace, France	+	R3189B
9	Middle Age	Molar tooth	Unknown/immature	Roeschwoog	−	R1051B
10	Twentieth century AD	Femur	Male/adult	War grave	−	

n.t. nontested for ancient DNA, "–" no genetic profile obtained, "+" partial genetic profile, "++" complete genetic profile

[a] Sample 4, 1800–1400 BC

[b] Samples 5 and 6, 3rd c. BC–2nd c. AD

Fig. 1 Geographical provenance of archeological skeletal samples

nylon membrane (0.45 μm, 25 mm) previously weighed. The filters were dried overnight at 55 °C, and then weighed after cooling at room temperature. The weight difference before and after filtration was used to determine the amount of insoluble proteinic fraction of the sample supposing the total dissolution of the mineral phase.

Chemical analyses run on the supernatants allowed us to determine the calcium and phosphate contents of the mineral phase, respectively via complexometry with EDTA and visible spectrophotometry (determination of the sum of PO_4^{3-} and HPO_4^{2-} ions, using the phospho-vanado-molybdenic method). Details on these chemical titrations have already been described previously [38, 39].

The eventual presence of secondary elements within the skeletal specimens was checked by EDX analyses using LEO435VP scanning electron microscope operated at 15 keV, 1.5 nA.

Powder X-ray diffraction (XRD) was used for crystallized phase identification using an INEL CPS 120 curved-counter diffractometer with the monochromatic CoKα radiation (λ_{Co}=1.78892 Å).

Fourier transform infrared (FTIR) spectroscopy analyses of the specimens were performed on a Perkin Elmer 1700 spectrometer (64 scans; resolution, 4 cm^{-1}), using the KBr pellet method. Different spectral features were then examined for gaining insight on relative amounts of chemical vibrating species and also for studying the local chemical environments of the ions constituting the mineral phase present in the specimens. In a preliminary step, the vibrational contribution of the collagenic fraction present in various residual amounts in the specimens was subtracted thanks to the OMNIC 8 software, using a typical bone collagen sample from our collection.

1. The presence of vibration bands attributable to carbonate species was used—in correlation with carbonate apatite standards for which the level of carbonation was previously checked by coulometry (UIC, Inc. CM 5014 coulometer with CM 5130 acidification unit)—to evaluate the amount of CO_3^{2-} ions associated to the apatite mineral. To this aim, the integrated intensity of the $\nu_3(CO_3)$ band (between 1,530 and 1,340 cm^{-1}) was divided by the integrated intensity of the $\nu_3(PO_4)$ domain between 1,230 and 890 and the obtained ratio was compared with the ones found for the standards. This analysis was especially made possible thanks to the preliminary subtraction of the collagen spectral contribution until zeroing the amide vibrations in the 1,930-to 1,215-cm^{-1} domain. The analytical reproducibility was checked by performing the same quantification method in triplicate. The standard deviation of the carbonate content evaluated for one sample on the same spectra ranges between 0.07 and 0.4.

2. The $\nu_2\nu_4(PO_4)$ band, a large absorption ranging from 400 to 800 cm^{-1}, was treated by spectral decomposition using the ORIGIN 8.1 software. After subtraction of the collagen residual absorption, the vibrational contribution of specific bands previously identified in nanocrystalline apatitic compounds was added in the mathematical fit, considering the overall absorption band as a sum of Lorentzian peaks (expect for the minor $\nu_2(PO_4)$ contribution which was more adequately fitted to a Gaussian curve). Data reported by Vandecandelaere et al. [36] as well as anterior studies [18, 22, 32, 40] served as starting point for the positioning of each contributing band existing in this spectral domain: at 470 cm^{-1} corresponding to $\nu_2(PO_4^{3-})$, 530–534 cm^{-1} (non-apatitic HPO_4^{2-}), 550 cm^{-1} (apatitic HPO_4^{2-}), 560/575 cm^{-1}/601 cm^{-1} (apatitic PO_4^{3-}), 617 cm^{-1} (non-apatitic PO_4^{3-}), 631 cm^{-1} ($\nu_L(OH^-)$), and 670 cm^{-1} (H_2O libration mode). Ratios of integrated intensities were then used to follow the evolution of each spectral contribution, taking the sum of apatitic phosphate bands as a reference.
3. The $\nu_3\nu_1(PO_4)$ band, expanding from 1,230 to 890 cm^{-1} was already shown [21] to be constituted by a large number of contributions for which the exact nature is still not well known. However, some contributions have been shown to be related to the more or less mature state of the apatite phase and to surface, non-apatitic, phosphates. Fourier self-deconvolution (OMNIC 8) was employed here to potentially amplify these contributions. To this aim, the parameters σ~22 cm^{-1} and k=2.1 (except for sample 3a, k=1.5) were used.

To facilitate the reading of this paper, Table 2 summarizes the principal parameters/indexes that will be followed along this manuscript, as well as their relationship with physicochemical properties.

Results and discussion

XRD analyses

XRD analyses were run on each specimen for phase identification (Fig. 2) as well as an evaluation of degrees of crystallinity. All samples were found to exhibit similar diffraction patterns, in which all peaks could be indexed in reference to the apatite structure (JCPDS card no. 09-432). No crystallized secondary phase was detected. For the sake of comparison, the patterns obtained on two previously characterized synthetic bone-mimicking apatites (1w-hac and 1w-hap) were also added in Fig. 2.

The mean dimensions of the crystallites have been evaluated from application of Scherrer's formula from the full-width at half maximum (FWHM) of the diffraction peaks (002) and (310). This led to an estimation of, respectively, the mean length of the crystals in *c*-axis, and an averaged response between width and thickness of the apatite crystals [36]. The crystallite dimensions of the skeletal specimens were found to range between 20 and 27 nm along the *c*-axis, and between 7 and 17 nm in perpendicular direction (width/thickness response). The presence of larger crystallites in teeth samples could be assessed, due to an additional enamel contribution, leading to modifications for both (002) and (310) responses. It was not possible, however, from the sole analysis of mean crystallite lengths to discriminate the samples according to their nature (bone or teeth) or their age. As previously described for synthetic apatites matured for various amounts of time (e.g., [41, 42]), the growth of the crystals along the c-axis is indeed often less significant in the differences observed upon aging of the crystals. A significantly greater effect was in contrast seen on the (310) FWHM, with values between 13 and 17 nm for teeth as opposed to significantly thinner (7–8.5 nm) for bone crystallites. The mean crystalline dimensions of the two synthetic samples (1w-hap and 1w-hac) have also been estimated in a similar way as above, leading to lengths/widths (in nanometers) of 24.3/8.8 and 15.7/4.9, respectively. It shows that the former sample could more adequately be used to mimic "physical" features of bone apatites (via similar particle size) whereas the latter (which is carbonated) could more adequately mimic their "chemical" features.

Figure 2 also points out differences in the resolution of XRD patterns, depending on the samples, and this observation may be related to different degrees of crystallinity. The quantification of crystallinity is a rather difficult task for such patterns corresponding to rather poorly organized systems. This difficulty lies especially in the multiplicity of influential factors including particle size and crystal disorder (e.g., presence of ion vacancies) [36]. Person et al. [43] have nonetheless proposed a crystallinity index (CI) based on peak selected heights: the existence of this index may indeed prove helpful for comparative purposes, and it has already been used for skeletal specimens (e.g., [43–45]). The value of CI was measured in the present work according to Person's procedure. The OriginPro 8 software was used to perform baseline correction between 31.5° and 50° (2θ values relative to the CoKα radiation) and to determine the heights H of the four diffraction peaks—ranging between 34.5° and 40.5°—with the following relationship:

$$CI = [H(202) + H(300) + H(112)]/H(211)$$

As may be expected, teeth samples were found to exhibit the highest CI values (0.27–0.37), compared with bone samples which were noticeably less well crystallized, with CI ranging from 0.02 to 0.11 (see values in Table 3). As predictable, the modern bone sample corresponds to the lowest CI. No significant difference among bone samples could however

Table 2 Summary of bone/teeth diagenetic indexes of apatite and collagen used in this work

Diagenetic indexes	Formulas	Measured property	References
XRD parameters			
CI	CI=[H(202)+H(300)+H(112)]/H(211)	Linked to the degree of crystallinity of calcium phosphate apatite	Person et al. [43]
FWHM (002) FWHM (310)	$L(\mathrm{hkl}) = \frac{0.94\lambda}{\cos\theta\sqrt{\Delta_{\mathrm{sample}}{}^2+\Delta_{HA}{}^2}}$ where Δ_{sample} and Δ_{HA} are the FWHM of the (hkl) peak for the sample and for sintered stoichiometric hydroxyapatite, respectively	Mean crystallite dimension in the considered dimension (*keeping in mind however that crystalline disorder may also affect XRD peak broadening*)	Scherrer [62]
FTIR parameters			
$\nu_3(CO_3)/\nu_3\nu_1(PO_4)$	A(1,530–1,330)/A(1,230–890)	Linked to the wt.% CO_3	This study
$\nu_3\nu_1(PO_4)$ analyzed via self-deconvolution (apodization)	"Peripheral" maxima (1,115/1,110 and 1,020 cm^{-1}) "Central" maxima (1,090/1,095 and 1,030 cm^{-1}	Mineral maturity as in poorly crystalline apatite (non-apatitic phosphates) Mineral maturity as in well-crystallized stoichiometric apatite (apatite phosphate)	Rey et al. [21], Paschalis et al. [63], Farlay et al. [52], and this study
$\nu_4(PO_4)$ analyzed via spectral decomposition (curve-fitting)	See formulae in text	Semiquantitative analysis of apatitic and non-apatitic HPO_4 and apatitic OH	Vandecandelaere et al. [36]
Coll/PO_4	A(1,720–1,600)/(1,220–900)	Linked to collagen content	Sosa et al. [35]
Other data relative to organic content			
% "CP"	Weight of residual matter after filtration of acid-dissolved material	Acid-insoluble organic matter content (mainly collagen part; +*possibly traces of residual mineral protected from acidic dissolution by the organic matrix*)	This study
Calcium and phosphate titrations			
Ca/P	Ca (mmol)/P (mmol)	Departure from stoichiometry (if lower then 1.67)	Elliott [64]
Ca/(P+C)	Ca (mmol)/(P (mmol)+C (mmol))		Drouet [65]

Numbers in parentheses give the approximate positions of the peaks/bands in radians or wavenumbers, respectively

CI crystallinity index, *H* height of XRD peaks, *A* area of the FTIR bands

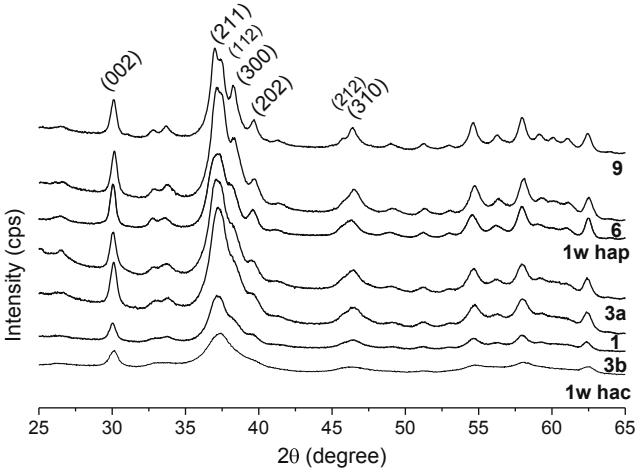

Fig. 2 XRD patterns of diagenetic samples no. 1 (modern/autopsy), no. 3a and 3b (outer and inner part of bone), no. 6 (Iron Age bone), and no. 9 (medieval teeth), as compared with a synthetic nanocrystalline apatite, maturation time of 1 week, carbonated (*1w-hac*), and noncarbonated (*1w-hap*). Line attribution according JCPDS 09-432 (apatite)

be determined: for instance, the Iron Age sample no. 4 exhibits the same CI value as sample no. 10, dating from the early twentieth century. These two samples have in contrast lower CI than the forensic samples no. 3a and 3b, which have experienced particular taphonomic history by staying 20 yrs in water. Our findings thus suggest that the taphonomic history, rather than age, appears as a particularly significant diagenetic parameter, affecting post mortem evolution of the biological apatite; and this is in perfect agreement with previous reports [43, 46].

At this point, it appeared interesting to seek potential correlations between these CI values and the previously estimated mean crystallite dimensions. Interestingly, a good correlation (R^2=0.96) was reached when plotting CI vs. crystallite widths (determined from (310) FWHM). As expected from our above findings, a significantly lower correlation was found (R^2=0.25) for CI vs. mean lengths.

Table 3 Synthesis of the quantitative and semiquantitative data arising from physicochemical characterization of modern, forensic, and archeological samples (bones and teeth)

No.	Epoch	% "CP"	Coll/PO_4	%CO_3 area ratio	Ca/P	Ca/(P+C)	CI	Adj R^{2a}	Formula[c]
1	Modern/autopsy	32.3	0.29	5.4	1.72	1.49	0.020	0.9984	$Ca_{8,9}\square_{1,1}(PO_4)_{4,9}(HPO_4)_{0,3}(CO_3)_{0,8}(OH)_{0,9}\square_{1,1}$
2	Modern/forensic	15.6	0.35	6.3	1.83	1.50	0.031	0.9986	$Ca_{9,0}\square_{1,0}(PO_4)_{5,0}(CO_3)_{1,0}(OH)_{1,0}\square_{1,0}$[b]
3a	Modern/forensic	23.2	0.35	6.6	1.48	1.33	0.043	0.9988	$Ca_{8,0}\square_{2,0}(PO_4)_{4,0}(HPO_4)_{1,4}(CO_3)_{0,7}\square_{2,0}$[b]
3b		33.6	0.30	4.8	1.58	1.39	0.044	0.9972	$Ca_{8,3}\square_{1,7}(PO_4)_{4,3}(HPO_4)_{1,0}(CO_3)_{0,7}(OH)_{0,3}\square_{1,7}$
4	Iron Age	n.a	0.38	5.3	1.62	1.37	0.038	n.a.	$Ca_{8,4}\square_{1,6}(PO_4)_{4,4}(HPO_4)_{0,8}(CO_3)_{0,8}(OH)_{0,4}\square_{1,6}$
5	Iron Age	28	0.27	7	1.82	1.51	0.107	0.9997	$Ca_{8,9}\square_{1,1}(PO_4)_{4,9}(CO_3)_{1,1}(OH)_{0,9}\square_{1,1}$
6	Iron Age	27.7	0.34	6.2	1.80	1.48	0.064	0.9971	$Ca_{9,1}\square_{0,9}(PO_4)_{5,1}(CO_3)_{1,0}(OH)_{1,1}\square_{0,9}$
7	IIIe–XIe s. av. JC	16	0.19	2.8	1.55	1.38	0.353	0.9993	$Ca_{8,6}\square_{1,4}(PO_4)_{4,6}(HPO_4)_{0,9}(CO_3)_{0,4}(OH)_{0,6}\square_{1,4}$
8	Middle Age	11.2	0.15	3.7	1.59	1.38	0.372	0.9995	$Ca_{8,6}\square_{1,4}(PO_4)_{4,6}(HPO_4)_{0,8}(CO_3)_{0,6}(OH)_{0,6}\square_{1,4}$
9	Middle Age	11.2	0.18	6.4	1.67	1.37	0.274	0.9997	$Ca_{8,4}\square_{1,6}(PO_4)_{4,4}(HPO_4)_{0,6}(CO_3)_{0,9}(OH)_{0,4}\square_{1,6}$
10	XXe s. ap. JC	n.a.	0.34	4.7	1.56	1.34	0.038	n.a.	$Ca_{8,3}\square_{1,7}(PO_4)_{4,3}(HPO_4)_{1,0}(CO_3)_{0,7}(OH)_{0,3}\square_{1,7}$

% "CP" fraction of acid-insoluble organic matter, considered as the collagenic part (CP) of the bone, *Coll/PO_4* ratio between areas under the curve of the amide I band of collagen (between 1,720 and 1,600 cm^{-1}) and of the $\nu_3\nu_1(PO_4)$ band (between 1,220 and 900 cm^{-1}), *%CO_3* area ratio (the reader is referred to the article content for detailed description), *CI* Cristallinity Index

[a] Adjusted R^2 coefficient resulting of the curve-fitting of the $\nu_4(PO_4)$ domain

[b] Corrected to avoid value <0

[c] Where the symbol "□" denotes an ion vacancy (either in Ca crystallographic sites or in OH sites)

FTIR spectroscopy analyses

Carbonate content

Direct estimation of the carbonate content by coulometry was not possible for the majority of samples studied here, given the low amount of available matter. The infrared signature of carbonate species was thus exploited to evaluate the samples carbonation level, after spectral subtraction of the collagen amide vibrations overlapping the carbonate domain $\nu_3(CO_3)$.

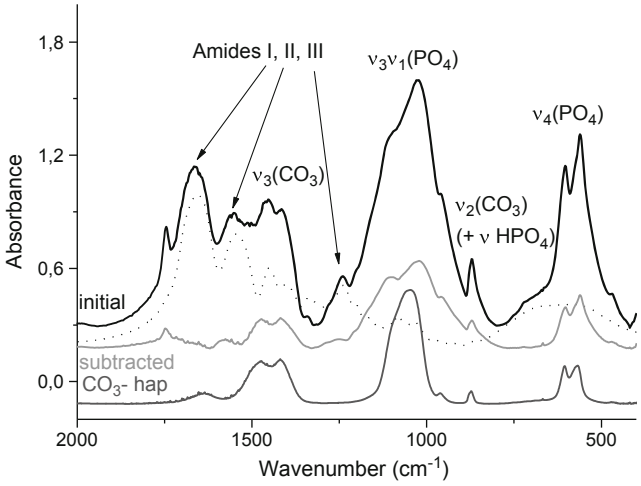

Fig. 3 Infrared spectra with band attribution. (1) Biological bone samples (sample no. 1, *black line*) showing both collagenic patterns and domains attributable to carbonated apatite, namely $\nu_3(CO_3)$, $\nu_3\nu_1(PO_4)$, $\nu_2(CO_3)$, and $\nu(HPO_4)$, $\nu_4\nu_2(PO_4)$. (2) Collagen sample (*dotted curve*), with indication of amides I, II, and III vibrations. (3) Example of a resulting spectrum (*light gray line*) after spectral subtraction of the collagen vibration bands. (4) Synthetic carbonated apatite (*dark gray line*) with 12 wt.% CO_3, showing only apatitic vibration bands

The spectral subtraction of the collagen domain then permitted to draw resulting spectra, which were judged satisfactory in terms of global appearance as compared with usual synthetic carbonated apatites (see Fig. 3). Interestingly, the $\nu_3\nu_1(PO_4)$ and $\nu_4(PO_4)$ domains were in fact only affected around the base of the absorption bands, without alteration of their general shape; these bands may thus be used for quantification purposes.

After the collagen spectrum subtraction process, the areas under the curve of the entire $\nu_3(CO_3)$ domain (range, 1,530–1,330 cm^{-1}) and of the $\nu_3\nu_1(PO_4)$ domain (between 1,230 and 890 cm^{-1}) were thus measured, as illustrated on Fig. 3. The carbonate-to-phosphate band area ratio was next quantitatively correlated with the carbonate content of the specimens, using a calibration curve built from separately prepared carbonated apatite standards (results to be published). By means of this method, the carbonate content of the diagenetic samples as well as of our modern reference specimen was evaluated. These carbonate contents were found to be comprised in the range 4–8 wt.% (Table 3), which is consistent with previous data on the carbonation rate of biological apatites [47–49]. An advantage of this method is that it is based on a comparison of bands area (integrated intensity) rather than on peak height (raw intensity). Moreover, in contrast to other FTIR-based ratio aiming at evaluating carbonate contents, the best correlation coefficient (R^2=0.9998) of the linear regression analysis is obtained when plotting the calculated area ratio $\nu_3(CO_3)/\nu_3\nu_1(PO_4)$ with the carbonate content of the apatite

standards. Other area ratios, previously used in other works [35, 45, 50], such as $v_3(CO_3)/v_4(PO_4)$ and $v_2(CO_3)/v_3v_1(PO_4)$, are found to be less correlated ($R^2=0.994$ and 0.864, respectively).

It may also be noted that a possible bias in such transmission FTIR-based carbonate quantifications could arise from the fact that they inform on average carbonate contents (global analysis) and do not refer to specific zones within each specimen. Indeed, Lebon et al. [46] has pointed out a great heterogeneity in carbonate content distribution among a given sample, especially around Haversian canals, where carbonate impurities may accumulate (thus with some carbonate ions not being solely incorporated into the apatite lattice).

Attempts have then been made to correlate these FTIR parameters with the XRD findings. Previous diagenetic studies [43, 46] found a correlation between CI values and the CO_3 content (the CO_3 content decreasing with increasing crystallinity). However, in the present work, no clear correlation existed between these two parameters, even if taking into account only bone samples (in order to avoid the contribution of enamel hydroxyapatite microcrystals in this estimation). These differing results may chiefly depend on the heterogeneity in the burial context of these bone specimens, whether terrestrial or aquatic, which could alter the specimens via various pathways. Diagenetic alteration of the CO_3 content is obviously site-specific [32, 51]. Moreover, observations on synthetic and diagenetic bone apatite (e.g., francolite) point toward agreement between high carbonate content and a high crystalline organization. In synthetic apatite compounds, CO_3 content tends to increase spontaneously along with the maturation of the crystals [32], by interacting with atmospheric carbon dioxide.

Investigation of the $v_3v_1(PO_4)$ domain (Fourier self-deconvolution)

Additional information on apatitic compounds may also be provided by focusing on the $v_3v_1(PO_4)$ domain, which may be considered as composed of a low-wavenumber component and a high-wavenumber component (splitting around 1,085–1,080 cm^{-1}). Tooth (Fig. 4c) and bone patterns (Fig. 4a, b) are well discriminated and resemble those of enamel and bone, as described by Rey et al. [21] respectively.

The low-wavenumber domain can be mainly described by two maxima at 1,030 and 1,020 cm^{-1}. The relative intensities of these two maxima have previously been correlated to the maturation degree of the sample [21], and the peak at 1,030 cm^{-1} becoming more significant for mature systems. No attempt has been made here to quantify the mineral maturation state based on the 1,030/1,020 intensity ratio, contrarily to ref. [35], nor the 1,030/1,110 cm^{-1} area ratio [52], as we noticed that the $v_3v_1(PO_4)$ domain was particularly sensitive to the nonuniform granulometry of the samples, thus leading to a lack of precision of the vibration domain [53]. Nonetheless, qualitative analysis of the spectra in this range provides valuable data about the maturation state of the samples. All diagenetic bone specimens studied here exhibited a maximum intensity at 1,030 cm^{-1}, with absorption at 1,020 cm^{-1} appearing as a shoulder, as described for well-mineralized enamel [21]. This observation is consistent with the general trend of the maturation process observed on biological and synthetic apatite [21]. Only the modern sample (sample no. 1, Fig. 4b), the closest to freshly precipitated apatite, exhibits a higher intensity at 1,020 cm^{-1}, which is attributed to phosphate ions in nonstoichiometric apatites and in the most immature synthetic apatites (type B carbonate and HPO_4^{2-}-containing apatites), thus probably indicating the persistence of vacancies. Intermediate profiles are obtained for forensic bone samples, exhibiting both maximum at 1,030 cm^{-1} and a clear band at 1,020 cm^{-1}. This hybrid pattern could be related on an intermediate state of maturation, or on a coexistence of well-crystallized and poorly crystalline materials within the same sample. At a microscopic level, diagenetic modifications may indeed vary within a given specimen [46]. However, the concordance of this 1,030/1,020 cm^{-1} pattern with the high collagenic content and the high DNA yield in sample no. 3b (Fig. 4a) is consistent with an exceptional preservation state of both organic and inorganic contents (potentially cooperating to protect each other from degradation factors). Among teeth samples, a slight difference is identified between the two medieval teeth (no. 8 and 9, Fig. 4c) with a larger contribution at 1,020 cm^{-1} for sample no. 9. This observation might be related to the more immature state of the latter, but anatomo-histological analyses would be required to confirm this conclusion. By contrast, the Chilean tooth powder (sample no. 7, Fig. 4c) exhibits similar features to fully mineralized enamel [21]. These results, obtained for teeth samples no. 7, 8, and 9, are in accordance with XRD data mentioned above, where greater CI values were obtained for samples no. 7 and 8 (respectively 0.35 and 0.37) as opposed to sample no. 9 (0.27).

In the high-wavenumber domain (1,150–1,080 cm^{-1}), the modern sample (sample no. 1, Fig. 4b) is characterized by a broad pattern composed of several maxima especially at around 1,115 and 1,095 cm^{-1}. In freshly precipitated synthetic apatites, a fairly large number of contributive bands have been pointed out in the literature [21]; whereas in biological apatites (bones and teeth), two main maxima at ~1,110 and 1,095 cm^{-1} were reported at the expense of other bands. In the present study, some variation in the relative intensities of the two maxima was noticed among the samples. For instance, among archeological bone specimens (Fig. 4b), samples no. 5 and 6 (Egyin Gol site) showed a more intense absorption at 1,095 cm^{-1}, in contrast to sample no. 4 (Krasnoyarsk site) exhibiting a more pronounced intensity at 1,115 cm^{-1}. For teeth samples (samples no. 7, 8, and 9, Fig. 4c), the absorption around 1,095 cm^{-1} is clearly dominant, despite a shift of the

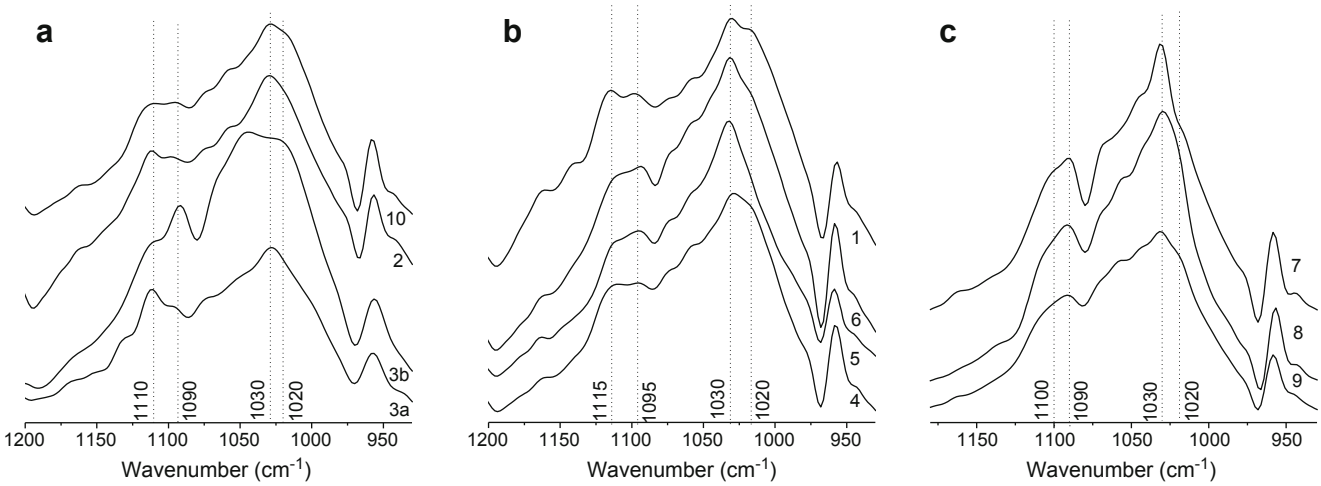

Fig. 4 FTIR patterns of $\nu_3\nu_1(PO_4)$ bone and teeth samples, after self-deconvolution posttreatment (Happ–Genzel apodization), exhibiting two distinct domains, in the low-wavenumber range (1,080–970 cm^{-1}) and in the high-wavenumber range (1,190–1,080 cm^{-1}). **a** Forensic bone samples and early twentieth century bone sample. **b** Modern and Iron Age bone samples. **c** Teeth samples

maximum from 1,095 to 1,090 cm^{-1}, probably due to the contribution of enamel [21]

The 1,110–1,115 cm^{-1} band has been shown to be correlated with non-apatitic phosphate environments contributing in the $\nu_4(PO_4)$ domain [21, 22]. However, a bias in the determination of the relative intensity of both 1,110–1,115 and 1,095 cm^{-1} could originate from the high carbonation rate of apatite, which is the case of our samples as previously mentioned. The carbonate content indeed tends to broaden the 1,095-cm^{-1} band with an eventual contribution in the ~1,110-cm^{-1} domain. Substitutions of phosphate by carbonate ions also tend to inhibit the maturation process of the crystals, which could promote the persistence of metastable phosphates in non-apatitic environments and therefore explain the presence of strong absorption at ~1,110 cm^{-1}. In samples no. 1 (Fig. 4b) and 10 (Fig. 4a), both 1,110 and 1,020 cm^{-1} absorptions are rather intense, which clearly indicates a low maturation state. Conversely, it is less straightforward to conclude about the ratio of these bands for the other forensic bone samples (e.g., samples no. 2 and 3a, Fig. 4a), exhibiting at the same time mature mineral feature (i.e., unique maximum at 1,030 cm^{-1} in the low-wavenumber range) and young mineral feature (i.e., intense band at ~1,110 cm^{-1}). This matter of fact might be assignable to existing heterogeneities within the specimens; also, the contribution of vibrations from organic contaminants for samples no. 2 and 3a cannot be excluded, which may be related to two domains on their FTIR spectra, in the range 3,000–2,800 cm^{-1} and in the range 1,600–1,500 cm^{-1} (see Fig. 6b).

Curve fitting in the $\nu_4(PO_4)$ domain

In order to draw complementary information on the apatitic phase contained in the diagenetic specimens analyzed in this work, the $\nu_4(PO_4)$ domain was also specifically explored. Considering the contribution of organic matter in the range 900–400 cm^{-1}, the investigation of the $\nu_4(PO_4)$ for our biological samples was performed after spectral subtraction of collagen (as was done above for the CO_3 content determination). We then applied the curve fitting protocol that was previously established for synthetic apatites [36], allowing one to identify apatitic and non-apatitic-phosphate environments as well as apatitic hydroxide ions. The adjusted *R*-square (adj. R^2) obtained after curve-fitting was systematically comprised between 0.997 and 1.000 (Table 3). A typical example of fitting result is shown on Fig. 5 (case of the tooth sample no. 7).

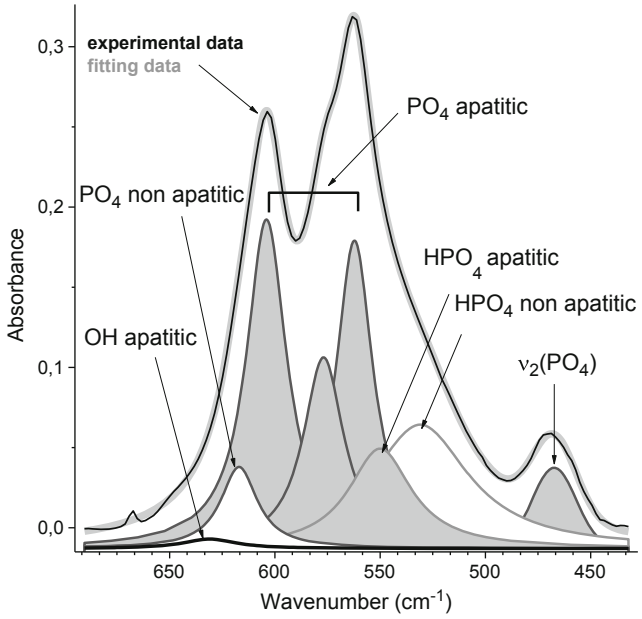

Fig. 5 Spectral decomposition of the $\nu_4(PO_4)$ infrared domain for teeth sample no. 7 with attribution of the different contributions. Except for the $\nu_2(PO_4)$, all curves are considered as Lorentzian

Insights on the maturation state of the apatite phase can in particular be assessed from the relative proportion of phosphate-bound vibrations assigned to non-apatitic environments (also called "labile") relatively to apatitic ones . The presence of apatitic OH^- ions can also be inferred (and bring valuable data on the composition and consequently on the stoichiometry of the apatite samples) from the observation of a contribution at 632 cm^{-1}.

Based on the integrated intensities obtained via curve fitting of this $\nu_4(PO_4)$ domain, we drew semiquantitative information about ionic species for which direct titration or analyses were impossible or delicate. The relative amount of such ionic species were expressed as a ratio of integrated intensities, respectively denoted R(OH), $R(HPO_4)_{ap}$ and $R(HPO_4)_{non}$ (ap for apatitic, non for non-apatitic), defined as:

$$R(\mathrm{OH}) = \frac{\mathrm{OH_{ap}}}{\mathrm{OH_{ap}} + \mathrm{PO_{4ap}} + \mathrm{HPO_{4ap}}}$$

$$R(\mathrm{HPO_4})_{non} = \frac{\mathrm{HPO_{4non}}}{\mathrm{PO_{4ap}} + \mathrm{PO_{4non}} + \mathrm{HPO_{4ap}} + \mathrm{HPO_{4non}}}$$

$$R(\mathrm{HPO_4})_{ap} = \frac{\mathrm{HPO_{4ap}}}{\mathrm{PO_{4ap}} + \mathrm{PO_{4non}} + \mathrm{HPO_{4ap}} + \mathrm{HPO_{4non}}}$$

On the basis of a previous work [54], a correlation study was performed by comparing these semiquantitative infrared data with XRD data, i.e., CI, (002) and (310) FWHM. Note that, in the following results, the data relative to sample no. 3b were not taken into account, this sample being found to depart from the general trend, possibly due to inadequate curve fitting indicated by a low adj. R^2.

Interestingly, a linear-like correlation (slope denoted "*a*") was found by plotting CI values against the R(OH), $R(HPO_4)_{ap}$, and $R(HPO_4)_{non}$ ratios, with R^2 ranging between 0.64 and 0.78 (see Table 4). The best correlation was found in the case of $R(HPO_4)_{non}$ relative to non-apatitic hydrogenphosphate groups, and the negative slope may indeed be expected (better crystallized systems being closer to stoichiometry, thus containing less non-apatitic ions). These findings strongly support the association existing between maturation and crystallinity state [52] within apatitic compounds, which is thus also applicable to diagenetic specimens. Indeed, the hydrated layer tends to disappear along with the maturation process, which is accompanied by an increase in crystallinity (degree of lattice organization).

Table 4 Summary of parameters of the linear fits (slope "*a*" and correlation coefficient R^2) obtained by plotting XRD data (columns), namely CI, (002) FWHM, and (310) FWHM, against FTIR intensity ratios from the $\nu_4(PO_4)$ domain, namely R(OH), R(HPO4)non, and R(HPO4)ap (rows)

Ratio of integrated intensities	R(OH)	$R(HPO_4)_{non}$	$R(HPO_4)_{ap}$
CI	a=0.36; R^2=0.6665	a=−0.73; R^2=0.7853	a=0.25; R^2=0.6423
(002) FWHM	a=−1.13; R^2=0.492	a=1.86; R^2=0.3896	a=−0.7; R^2=0.3743
(310) FWHM	a=−0.18; R^2=0.7204	a=0.31; R^2=0.6532	a=−0.1; R^2=0.3578

In contrast to Miller et al., no clear correlation was evidenced between FWHM of the (002) diffraction line and acid phosphate content (R^2<0.4), and between (002) FWHM and OH content (R^2~0.5). As mentioned previously, the (002) widths seem to be a less discriminative parameter than the (310) widths to assess the crystallinity state of our samples. For the latter, R^2 values are found to be higher in correlation analyses of R(OH) and $(HPO_4)_{non\text{-}apatitic}$, respectively 0.7 and 0.65, but an equally poor relationship is found for apatitic HPO_4 ratio. One shall consider that apatitic hydrogenphosphates are less representative of the maturation process, as these species do not belong to the hydrated layer. By contrast, due to the importance of substitutions in trivalent anionic site by bivalent ions (CO_3^{2-} and HPO_4^{2-}), compensated by vacancies in the OH site, the presence of hydroxide ions are a well-known feature of better crystallized apatites.

These correlative XRD/FTIR results may thus be seen as a validation of our spectral decomposition protocol (with spectral subtraction of collagen). The positive or negative sign of the various slopes "*a*" found in Table 4 are perfectly consistent with expected relationships between crystallinity and maturity state.

Chemical analyses

Estimation of the organic content

The organic content contained in most specimens was estimated by weighing the acid-insoluble fraction of the samples collected during filtering. Theoretically, the insoluble phase is thought to represent only organic material and, in particular, the collagenic part (CP) of the tissue. Nonetheless, the solutions aspects before filtration were evocating a complex mixture of gelatinous compound and other impurities. This gravimetric analysis was however performed to draw a first approximation of the organic content within the samples.

As summarized in Table 3, the supposed organic fraction (% CP) was found to account for 11.2 to 33.6 wt.% of the samples, with no clear dependence with the age of the sample. The organic fractions of the teeth samples (11–16 wt.%) were, as expected, low compared with most bone specimens because the teeth powders included dentin and cementum materials but also enamel, the latter containing minute amount of organic material. The lower values of organic amounts observed for some bone samples (e.g., no. 2 and 3a) are consistent with the loss of organic matter preferentially degraded during early diagenesis stages, in relation to the initial

proportions of the collagen part into these skeletal samples. Instead, the modern "reference" bone no. 1—sampled after autopsy and stored frozen—, exhibits a value of ~32 wt.%, corresponding to the expected value for a modern compact bone sample. It is not surprising to find rather similar organic contents for the "old" samples from Egyin Gol site in Mongolia, where good preservation conditions were assured. It points in particular to the crucial role of environmental temperature in the preservation of the sample. The degradation of the specimen is probably more dependent on the initial postmortem conditions than on datation itself. Also, the surface of a sample may become more degraded than internal parts due to direct contact with surrounding media (this can for example explain the difference observed between samples 3a and 3b). The lowest bone organic fraction is found in this study for the forensic sample no. 2 which experienced very drastic diagenetic conditions, evidenced by a visible surface decomposition of the femoral specimen. The effect of temperature has also been discussed in the scope of ancient DNA studies [55]. Although successful DNA retrieval could be achieved for samples which have remained in cold to temperate environments (as for the Roeschwoog teeth, sample no. 8), ancient DNA extraction generally failed for hot climate field studies (e.g., the tooth of Solcor, sample no. 7), even though organic matter seemed to be preserved. The discrepancy noticed for ancient DNA availability between the two Mongolian samples (samples no. 5 and 6) illustrates that temperature is however not the only factor involved in DNA degradation. In addition, the preservation conditions (temperature, pH, and ionic strength) can modify the type of interaction that DNA molecules may establish with the apatitic mineral, as we recently pointed out [29].

At this point, it was interesting to check whether this rough estimation of organic content (based on gravimetric evaluation) could be correlated to the amount of collagen observable by FTIR. To do so, the relative amount of collagen was semiquantitatively followed, as proposed earlier [35, 46], by determining the area ratio between the amide I band of collagen at 1,720–1,600 cm^{-1} and the $\nu_3\nu_1(PO_4)$ band in the range 1,220–900 cm^{-1} (see Coll/PO_4 ratio on Table 3). As a whole, the plot of % CP versus Coll/PO_4 only led to a poor linear correlation (R^2~0.36). However, among the datapoints lying out of the line are the two samples (no. 2 and 3a), which were exposed to surface alterations (thus potentially prone to organic contamination), for which FTIR spectra indicate (e.g., in the range 3,000–2,800 and 1,600–1,500 cm^{-1}, see Fig. 6) the presence of additional organic matter, most probably in the form of fat matter/lipids. Interestingly, a significantly improved correlation was reached without these two points (R^2~0.96), thus supporting the gravimetry/FTIR interrelated conclusions on the evolution of organic matter contents (Fig. 6a).

Composition of apatite samples

By means of chemical titrations of calcium ions and phosphate ions in the mother solutions obtained after acidic dissolution, the Ca/P ratios of the samples were experimentally determined, and found between 1.48 and 1.83 (Table 3). We next attempted to determine the general apatite formulas of our samples by associating those Ca/P values with the FTIR-based carbonate contents. Using this system of two equations with two unknown parameters (i.e., the HPO_4^{2-} and the CO_3^{2-} contents), we were then able to estimate averaged chemical formulas for each sample (see Table 3), and to evaluate in particular the corresponding Ca/(P+C) ratios, which ranged between 1.33 and 1.53. This range falls below the theoretical stoichiometric value of 1.67, which points out the nonstoichiometry of the apatitic phase contained in these samples and which is consistent with the general formulae of bony apatite proposed by R. Legros for cortical bone apatite [56]: $Ca_{8.3}\square_{1.7}(PO_4)_{4.3}(HPO_4, CO_3)_{1.7}(OH)_{0.3}\square_{1.7}$ (giving an average Ca/(P+C) ratio of 1.38 and considering carbonate substitution mainly in B-site).

The chemical formula estimated here also point out the presence of non-negligible HPO_4^{2-} contents (substituting PO_4^{3-} ions beside carbonate), which were indeed detected above by FTIR. The estimated amounts of hydroxide ions OH^- are found to be rather low (typically lower than 1.1 per unit formula). These observations illustrate the nonstoichiometry of these bioapatite minerals. The substitution of PO_4^{3-} ions by HPO_4^{2-} or CO_3^{2-} and the lack of OH^- anions are, from an electroneutrality point of view, accounted for by the existence of cationic and anionic vacancies (in Ca− and OH− sites, respectively). The persistence of ion vacancies in the lattice is a well-known phenomenon, which has also been described for synthetic apatites even after a long period of maturation [57].

In addition to calcium, phosphate, carbonate and hydroxide ions, which represent the main ionic components of biological apatites, the more minor contribution of other cations in the lattice (which have not been quantified here) may however also be pointed out. Indeed, the MEB-EDS analyses evidenced the presence of magnesium in most of the samples, as well as sodium and aluminum. Trace amounts of other cationic species were also detected in some samples (strontium, iron, potassium). These elements may either be incorporated in the apatitic lattice as substituents or may be present as minor secondary phases, although no foreign crystalline phase was detected by XRD analysis. Indeed, the presence of surface contaminants cannot be strictly ruled out for such diagenetic specimens. From a physicochemical point of view, the enrichment of apatite with foreign ions (especially bivalent), e.g., via surface ion exchange in solution, has been pointed out for example in the case of Sr^{2+} or Mg^{2+} [57, 58], whereas monovalent cations like K^+ and Na^+ tend to

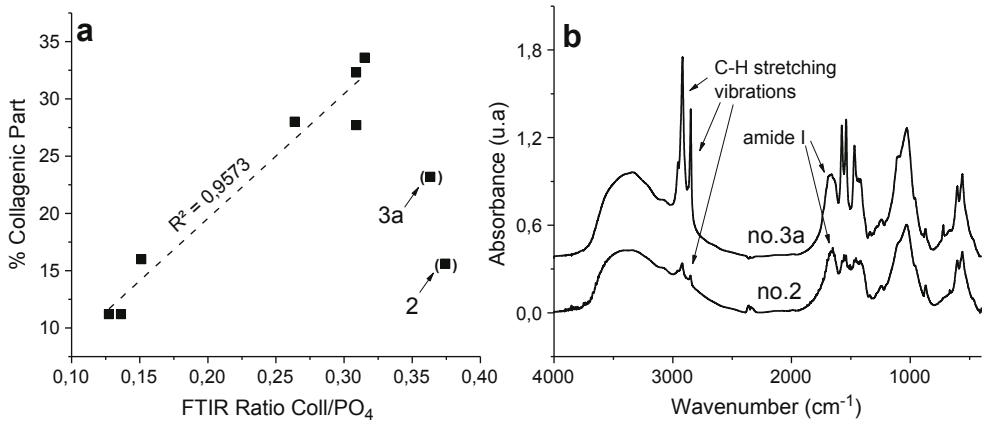

Fig. 6 **a** Correlation between gravimetric method (*%CP*) and FTIR method (Ratio Coll/PO4) to determine the organic content of skeletal samples. Two samples are considered as outliers (no. 2 and 3a). **b** FTIR spectra of outlier samples showing additional vibrations attributable to organic matter (in the range 3,000–2,800 and 1,600–1,500 cm^{-1})

contribute less [57]. Physiological Mg^{2+} was found to be incorporated into dentin and enamel tissues in about 0.5–1 wt.% [59], and generally speaking the chemical composition of mineralized tissues depends on that of the surrounding aqueous environment (whether physiological or diagenetic milieu). This potential incorporation of exogenous cations could also be balanced by anionic species; the main contribution allegedly being in the form of sulfate or silicate anions. Surprisingly, only few elements conventionally described as substitution elements in OH-site are detected (i.e., fluoride and chloride ions are present respectively in the Russian sample no. 4 and the Chilean sample no. 7).

Concluding statements

The analytical approach used in this work has been optimized for the study of diagenetic specimens, according to mathematical posttreatments of data, which are not liable to alter significantly the original features of the samples. Diagenesis, as well as chemical pretreatment, may impact both the organic (collagenic) matter and apatite nanocrystals, whose surface is known to be in a metastable equilibrium with the surrounding environment. By means of correlation analysis, we were able to determine a consistent set of qualitative indexes (patterns in the infrared $\nu_3\nu_1(PO_4)$ domain after apodization), either semi-quantitative (XRD CI, FTIR determination of ionic species, e.g., non-apatitic HPO_4 and apatitic OH) or quantitative (carbonate content, organic matter estimation). These indexes provide information on the nature, the crystallinity degree and the maturation state of the samples. The results of this study appear to be representative of the general state of conservation by comparing these diagenetic features to those of a reference modern bone. Therefore, it allows to better apprehend the diagenetic alteration of the original biological apatite originating from bone and teeth specimens usable as ancient DNA substrate. Indeed, previous seminal works are in agreement with the fundamental role of apatite in the preservation of ancient DNA within skeletal remains.

These results are in global accordance with previous diagenetic works. The positive effect of low temperature environment is assessed, given the location of three of the four specimens allowing DNA amplification (Roeschwoog, Krasnoyiarsk, Egyin Gol). These specimens all exhibit distinct physicochemical features (in terms of maturation, crystallinity, and organic content), thus suggesting involvement of a complex equilibrium at stake in DNA preservation, balanced between crystallinity increase and preservation of the original signature of biological, poorly crystallized, apatite nanocrystals. On the one hand, diagenetic evolution of apatite towards well-crystallized and well-maturated nanocrystals leads apatite to reach a stability state, which was recently demonstrated by calorimetry [16], allowing it to persist over a wide time range. On the other hand, this phenomenon may be increased in the case of dissolution/crystallization events, which could also alter the molecular content of the specimens, especially when these processes are linked with microorganisms activity. Results are easier to discuss when organic contaminants are detectable at the surface of a bone specimen due to drastic diagenetic conditions (e.g., aquatic environment). Deeper sampling in such bone specimens has in contrast been shown to exempt of such exogenous material. In this particular case, not a single molecule of ancient DNA from the outer part of bone succeeded to be amplified, whereas a full DNA profile was obtained from the inner part.

Considering the scarcity of the studied samples and their variability (age, geographical provenance, and type of burial site), no attempt has been made at this stage to correlate these results with DNA preservation. However, the multi-analytical approach deployed in this work is intended to be applied to a broader set of samples, and could thus prove useful to correlate in a more general way diagenetic physicochemical parameters with the presence of DNA within skeletal specimens. Additional diagenetic parameters could also prove helpful for even further understanding preservation mechanisms allowing DNA persistence (e.g., trace elements analyses and sediments analyses).

Acknowledgments This research was supported by the Institute of Ecology and Environment (INEE) and the Institute of Chemistry (INC) of the French National Center for Scientific Research (CNRS).

References

1. Tütken T, Vennemann TW (2011) Fossil bones and teeth: preservation or alteration of biogenic compositions? Palaeogeogr Palaeoclimatol Palaeoecol 310:1–8. doi:10.1016/j.palaeo.2011.06.020
2. Price TD, Schoeninger MJ, Armelagos GJ (1985) Bone chemistry and past behavior: an overview. J Hum Evol 14:419–447
3. Lee-Thorp JA (2008) On isotopes and old bones. Archaeometry 50: 925–950. doi:10.1111/j.1475-4754.2008.00441.x
4. Keyser-Tracqui C, Ludes B (2005) Methods for the study of ancient DNA. Methods Mol Biol 297:253–264
5. Rohland N, Hofreiter M (2007) Ancient DNA extraction from bones and teeth. Nat Protoc 2:1756–1762. doi:10.1038/nprot.2007.247
6. Ostrom PH, Schall M, Gandhi H, Shen TL, Hauschka PV, Strahler JR, Gage DA (2000) New strategies for characterizing ancient proteins using matrix-assisted laser desorption ionization mass spectrometry. Geochim Cosmochim Acta 64:1043–1050. doi:10.1016/S0016-7037(99)00381-6
7. Buckley M, Anderung C, Penkman K, Raney BJ, Gotherstrom A, Thomas-Oates J, Collins MJ (2008) Comparing the survival of osteocalcin and mtDNA in archaeological bone from four European sites. J Archaeol Sci 35:1756–1764. doi:10.1016/j.jas.2007.11.022
8. Keyser C, Bouakaze C, Crubézy E, Nikolaev VG, Montagnon D, Reis T, Ludes B (2009) Ancient DNA provides new insights into the history of south Siberian Kurgan people. Hum Genet 126:395–410. doi:10.1007/s00439-009-0683-0
9. Amory S, Huel R, Bilić A, Loreille O, Parsons TJ (2012) Automatable full demineralization DNA extraction procedure from degraded skeletal remains. Forensic Sci Int: Genet 6:398–406. doi:10.1016/j.fsigen.2011.08.004
10. Orlando L, Ginolhac A, Zhang G et al (2013) Recalibrating Equus evolution using the genome sequence of an early Middle Pleistocene horse. Nature 499:74–78. doi:10.1038/nature12323
11. Pääbo S, Poinar H, Serre D, Jaenicke-Despres V, Hebler J, Rohland N, Kuch M, Krause J, Vigilant L, Hofreiter M (2004) Genetic analyses from ancient DNA. Annu Rev Genet 38:645–679. doi:10.1146/annurev.genet.37.110801.143214
12. Campos PF, Craig OE, Turner-Walker G, Peacock E, Willerslev E, Gilbert MTP (2012) DNA in ancient bone—where is it located and how should we extract it? Ann Anat-Anat Anz 194:7–16. doi:10.1016/j.aanat.2011.07.003
13. Adler CJ, Haak W, Donlon D, Cooper A (2011) Survival and recovery of DNA from ancient teeth and bones. J Archaeol Sci 38:956–964. doi:10.1016/j.jas.2010.11.010
14. Higgins D, Austin JJ (2013) Teeth as a source of DNA for forensic identification of human remains: a review. Sci Justice 53:433–441. doi:10.1016/j.scijus.2013.06.001
15. Gilbert MTP, Willerslev E, Hansen AJ, Barnes I, Rudbeck L, Lynnerup N, Cooper A (2003) Distribution patterns of postmortem damage in human mitochondrial DNA. Am J Hum Genet 72:32–47
16. Rollin-Martinet S, Navrotsky A, Champion E, Grossin D, Drouet C (2013) Thermodynamic basis for evolution of apatite in calcified tissues. Am Mineral 98:2037–2045. doi:10.2138/am.2013.4537
17. Eanes ED, Meyer JL (1977) The maturation of crystalline calcium phosphates in aqueous suspensions at physiologic pH. Calc Tis Res 23:259–269. doi:10.1007/BF02012795
18. Rey C, Hina A, Tofighi A, Glimcher MJ (1995) Maturation of poorly crystalline apatites: chemical and structural aspects in vivo and in vitro. Cells Mat 5:345–356
19. Rey C, Lian J, Grynpas M, Shapiro F, Zylberberg L, Glimcher MJ (1989) Non-apatitic environments in bone mineral: FT-IR detection, biological properties and changes in several disease states. Connect Tissue Res 21:267–273
20. Combes C, Rey C, Eichert D, Drouet C (2005) Formation and evolution of hydrated surface layers of apatites. Key Eng Mater 284:3–6
21. Rey C, Shimizu M, Collins B, Glimcher MJ (1991) Resolution-enhanced Fourier transform infrared spectroscopy study of the environment of phosphate ion in the early deposits of a solid phase of calcium phosphate in bone and enamel and their evolution with age: 2. Investigations in the ν_3 PO_4 domain. Calcif Tissue Int 49:383–388
22. Rey C, Shimizu M, Collins B, Glimcher MJ (1990) Resolution-enhanced Fourier transform infrared spectroscopy study of the environment of phosphate ions in the early deposits of a solid phase of calcium-phosphate in bone and enamel, and their evolution with age. I. Investigations in the ν_4 PO_4 domain. Calcif Tissue Int 46:384–394
23. Cazalbou S, Eichert D, Ranz X, Drouet C, Combes C, Harmand MF, Rey C (2005) Ion exchanges in apatites for biomedical application. J Mater Sci Mater Med 16:405–409. doi:10.1007/s10856-005-6979-2
24. Errassifi F, Menbaoui A, Autefage H et al (2010) Adsorption on apatitic calcium phosphates: applications to drug delivery. In: Narayan R, McKittrick J (eds) Advances in bioceramics and biotechnologies. Amer Ceramic Soc, Westerville, pp 159–174
25. Ouizat S, Barroug A, Legrouri A, Rey C (1999) Adsorption of bovine serum albumin on poorly crystalline apatite: influence of maturation. Mater Res Bull 34:2279–2289. doi:10.1016/S0025-5408(00)00167-7
26. Posner AS (1985) The structure of bone apatite surfaces. J Biomed Mater Res 19:241–250. doi:10.1002/jbm.820190307
27. Drouet C, Carayon MT, Combes C, Rey C (2005) Exchange of biologically relevant ions on nanocrystalline apatites. Geochim Cosmochim Acta 69:A69–A69
28. Lindahl T (1993) Instability and decay of the primary structure of DNA. Nature 362:709–715. doi:10.1038/362709a0
29. Grunenwald A, Keyser C, Sautereau A-M, Crubézy E, Ludes B, Drouet C (2014) Adsorption of DNA on biomimetic apatites: towards the understanding of the role of bone and tooth mineral on the preservation of ancient DNA. Appl Surf Sci 292:867–875. doi:10.1016/j.apsusc.2013.12.063
30. Götherström A, Collins MJ, Angerbjörn A, Lidén K (2002) Bone preservation and DNA amplification. Archaeometry 44:395–404. doi:10.1111/1475-4754.00072
31. Hagelberg E, Bell LS, Allen T, Boyde A, Jones SJ, Clegg JB (1991) Analysis of ancient bone DNA: techniques and applications [and discussion]. Philos Trans R Soc Lond Ser B Biol Sci 333:399–407
32. Cazalbou S, Eichert D, Drouet C, Combes C, Rey C (2004) Minéralisations biologiques à base de phosphate de calcium. Comptes Rendus Palevol 3:563–572. doi:10.1016/j.crpv.2004.07.003
33. Trueman CN, Palmer MR, Field J, Privat K, Ludgate N, Chavagnac V, Eberth DA, Cifelli R, Rogers RR (2008) Comparing rates of recrystallisation and the potential for preservation of biomolecules from the distribution of trace elements in fossil bones. Comptes Rendus Palevol 7:145–158. doi:10.1016/j.crpv.2008.02.006
34. Yi H, Balan E, Gervais C et al (2013) A carbonate-fluoride defect model for carbonate-rich fluorapatite. Am Mineral 98:1066–1069. doi:10.2138/am.2013.4445
35. Sosa C, Vispe E, Núñez C, Baeta M, Casalod Y, Bolea M, Hedges REM, Martinez-Jarreta B (2013) Association between ancient bone preservation and DNA yield: a multidisciplinary approach. Am J Phys Anthropol 151:102–109. doi:10.1002/ajpa.22262

36. Vandecandelaere N, Rey C, Drouet C (2012) Biomimetic apatite-based biomaterials: on the critical impact of synthesis and post-synthesis parameters. J Mater Sci Mater Med 23:2593–2606. doi:10.1007/s10856-012-4719-y
37. Mendisco F, Keyser C, Hollard C et al (2011) Application of the iPLEXTM Gold SNP genotyping method for the analysis of Amerindian ancient DNA samples: benefits for ancient population studies. Electrophoresis 32:386–393. doi:10.1002/elps.201000483
38. Gee A, Deitz VR (1953) Determination of phosphate by differential spectrophotometry. Anal Chem 25:1320–1324. doi:10.1021/ac60081a006
39. Charlot G (1963) L'analyse qualitative et les réactions en solution. Masson, 1963, Paris, France
40. Kauppinen JK, Moffatt DJ, Mantsch HH, Cameron DG (1981) Fourier self-deconvolution: a method for resolving intrinsically overlapped bands. Appl Spectrosc 35:271–276
41. Vandecandelaère N (2012) Élaboration et caractérisation de biomatériaux osseux innovants à base d'apatites phospho-calciques dopées. INPT
42. Rowles S (1965) Studies on non-stoichiometric apatites. In: Stack MV, Fearnhead RW (eds) Tooth enamel: its composition, properties and fundamental structure. John Wright et Sons LTD, Bristol, Royaume-Uni, pp 23–25, 56–57
43. Person A, Bocherens H, Saliège J-F, Paris F, Zeitoun V, Gerard M (1995) Early diagenetic evolution of bone phosphate: an X-ray diffractometry analysis. J Archaeol Sci 22:211–221. doi:10.1006/jasc.1995.0023
44. Thompson TJU, Islam M, Piduru K, Marcel A (2011) An investigation into the internal and external variables acting on crystallinity index using Fourier transform infrared spectroscopy on unaltered and burned bone. Palaeogeogr Palaeoclimatol Palaeoecol 299:168–174. doi:10.1016/j.palaeo.2010.10.044
45. Pucéat E, Reynard B, Lécuyer C (2004) Can crystallinity be used to determine the degree of chemical alteration of biogenic apatites? Chem Geol 205:83–97. doi:10.1016/j.chemgeo.2003.12.014
46. Lebon M, Müller K, Bellot-Gurlet L, et al. (2012) Application des micro-spectrométries infrarouge et Raman à l'étude des processus diagénétiques altérant les ossements paléolithiques. ArchéoSciences no. 35:179–190
47. McElderry J-DP, Zhu P, Mroue KH et al (2013) Crystallinity and compositional changes in carbonated apatites: evidence from 31P solid-state NMR, Raman, and AFM analysis. J Solid State Chem 206:192–198. doi:10.1016/j.jssc.2013.08.011
48. Sader MS, Lewis K, Soares GA, LeGeros RZ (2013) Simultaneous incorporation of magnesium and carbonate in apatite: effect on physico-chemical properties. Mater Res 16:779–784. doi:10.1590/S1516-14392013005000046
49. LeGeros RZ (1991) Calcium phosphates in oral biology and medicine. Monogr Oral Sci 15:1–201
50. Boskey AL, Mendelsohn R (2005) Infrared spectroscopic characterization of mineralized tissues. Vib Spectrosc 38:107–114. doi:10.1016/j.vibspec.2005.02.015
51. Trueman CN, Privat K, Field J (2008) Why do crystallinity values fail to predict the extent of diagenetic alteration of bone mineral? Palaeogeogr Palaeoclimatol Palaeoecol 266:160–167. doi:10.1016/j.palaeo.2008.03.038
52. Farlay D, Panczer G, Rey C, Delmas PD, Boivin G (2010) Mineral maturity and crystallinity index are distinct characteristics of bone mineral. J Bone Miner Metab 28:433–445. doi:10.1007/s00774-009-0146-7
53. Trueman CN (2013) Chemical taphonomy of biomineralized tissues. Palaeontology 56:475–486. doi:10.1111/pala.12041
54. Miller LM, Vairavamurthy V, Chance MR, Mendelsohn R, Paschalis EP, Betts F, Boskey AL (2001) In situ analysis of mineral content and crystallinity in bone using infrared micro-spectroscopy of the v(4) PO43-vibration. Biochimica et Biophysica Acta (BBA)-General Subjects 1527:11–19
55. Smith CI, Chamberlain AT, Riley MS, Stringer C, Collins MJ (2003) The thermal history of human fossils and the likelihood of successful DNA amplification. J Hum Evol 45:203–217. doi:10.1016/S0047-2484(03)00106-4
56. Legros R, Balmain N, Bonel G (1986) Structure and Composition of the Mineral Phase of Periosteal Bone. J Chem Res-S 8–9
57. Cazalbou S (2000) Échanges cationiques impliquant des apatites nanocristallines analogues au minéral osseux. Thèse de doctorat, Institut national polytechnique
58. Drouet C, Carayon M-T, Combes C, Rey C (2008) Surface enrichment of biomimetic apatites with biologically-active ions Mg2+ and Sr2+: a preamble to the activation of bone repair materials. Mater Sci Eng C-Biomimetic Supramol Syst 28:1544–1550. doi:10.1016/j.msec.2008.04.011
59. Lefevre R, Frank RM, Voegel JC (1975) The study of human dentine with secondary ion microscopy and electron diffraction. Calcif Tissue Res 19:251–261
60. Keyser-Tracqui C, Crubezy E, Ludes B (2003) Nuclear and mitochondrial DNA analysis of a 2,000-year-old necropolis in the Egyin Gol Valley of Mongolia. Am J Hum Genet 73:247–260
61. Mendisco F (2011) Apports de la paléogénétique à l'histoire du peuplement précolombien des Andes méridionales (Vème–XVème siècles). Université de Toulouse, Université Toulouse III-Paul Sabatier
62. Scherrer P (1981) Estimation of the size and internal structure of colloidal particles by means of Rontgen rays. Nachr. Ges. Wiss., Gotengen 2:96–100
63. Paschalis EP et al. (1997) FTIR microspectroscopic analysis of normal human cortical and tribecular bone. Calcif. Tis. Int. 61(6): 480–486
64. Elliott JC (1994) Structure and chemistry of the apatites and other calcium orthophosphtes. Elsevier Science BV, Amsterdam
65. Drouet C (2013) Apatite formation: why it may not work as planned, and how to conclusively identify apatite compounds. BioMed Res. Ins., p. 490946. Doi:10.1155/2013/490946